European Journal of Mechanics / B Fluids 95 (2022) 194–204

Contents lists available at ScienceDirect

European Journal of Mechanics / B Fluids

journal homepage: www.elsevier.com/locate/ejmflu

Modeling and simulation of multi-component immiscible flows based on a modified Cahn–Hilliard equation

Qing Xia [a], Junseok Kim [b], Yibao Li [a,*]

[a] School of Mathematics and Statistics, Xi'an Jiaotong University, Xi'an 710049, China
[b] Department of Mathematics, Korea University, Seoul 02841, Republic of Korea

ARTICLE INFO

Article history:
Received 7 March 2022
Received in revised form 21 April 2022
Accepted 30 April 2022
Available online 11 May 2022

Keywords:
Multi-component flow
Navier–Stokes equation
Cahn–Hilliard model
Hyperbolic tangent property

ABSTRACT

In this study, an efficient method will be developed for the phase-field model of multi-component immiscible phases. The formulation of surface tension requires the interfaces to satisfy the hyperbolic tangent property. However, the interfacial transitions between different phases are not hyperbolic tangent profiles. The enclosed area is not preserved although the total mass is conserved by the original Cahn–Hilliard equation. This study is an extended research based on our previous study (Li et al., 2016). This work aims to apply the modified Cahn–Hilliard model into the multi-phase system. The interface is forced to be hyperbolic tangent by the modified Cahn–Hilliard system. The computational accuracy of the surface tension is improved under our multiphase framework. The mass loss of each phase can be reduced and the enclosed area can be preserved by the proposed method. We show various numerical results to demonstrate the robustness of the proposed modified model.

1. Introduction

The interface behavior between different phases is compromised by the viscosity, velocity and density of each component [1,2]. This phenomenon widely exists in a wide range of biomedical, physical and chemical processes, has been extensively studied through different interface capturing/tracking methods [3–6]. For example, emulsion produced by mixing two immiscible fluids, plays significant roles in various types of applications such as drug delivery and pharmacology research [7], multiphase physical field coupling simulation [8,9] and fusion of chemical factors [10–12]. Cahn–Hilliard(CH) equation has been proposed of spinodal decomposition for a binary alloy and usually used to describe the physical interfaces between heterogeneous phases [13]. Although the original CH equation can satisfy basic physical property, properties such as hyperbolic tangent and conservation of enclosing area cannot be satisfied. The hyperbolic tangent property can be viewed as a singular limit of the phase field equations for phase transitions [14,15], while there is a few research focus on this feature. Therefore, it is necessary to modify the original model to satisfy the requirements without changing the original characteristics.

How to develop an efficient numerical method for the multi-component immiscible flows has attracted widespread attention. Nichols et al. [16,17] proposed a volume-of-fluid model for determining the location of interfaces in multi-component materials by the volume fraction. Francois and Shyy [18] presented the immersed boundary method, which had been proved of high efficiency by selecting binary-fluid flow with kinds of fluid properties. This method avoided the problem of generating a body conformal grid and greatly improved the efficiency of computation [19–21]. The level set method is a popular computational technique to track moving interfaces between multiphase flows [22], which gets smooth results without sharp faults by using an implicit interface as a zero-level set of the auxiliary functional [23]. However, mass conservation of multi-component systems could not be guaranteed under this framework. Lowengrub and Truskinovsky [24] proposed a phase-field model coupled with multiple fluids with different densities. This method had been widely used for simulating the state and dynamical behavior of multiphase flows. Under their framework, the thin thickness transition regions were obtained with the condition of mass conservation and energy dissipation by introducing a conserved order parameter. Kim et al. [25–27] applied a modified phase-field model to simulate arbitrary combination of interfaces between different phases. In their work, a conservative multigrid method for the ternary CH system was established with second-order accuracy and unconditional stability.

This paper will describe the design and implementation of a multi-component phase-field model with a modified multi-component CH equation under the hydrodynamic framework. Due to the convection terms of the fluids, the interfacial transition between multiple phases is not hyperbolic, which is significant

* Corresponding author.
E-mail addresses: cfdkim@korea.ac.kr (J. Kim), yibaoli@xjtu.edu.cn (Y. Li).

https://doi.org/10.1016/j.euromechflu.2022.04.013
0997-7546/

for the calculation of the surface tension and leads to the non-conservation of the area of the closed area. To address these shortcomings, a fidelity term will be added to the original CH model. The interfacial transition can be represented by a explicit smoothing flow. The modified CH model forces the interface to satisfy the hyperbolic tangent property and significantly reduced the mass loss of each phase. Furthermore, the surface tension can be computed accurately by the modified CH model and the computation is not influenced by the over-determined issue. The discretization of the coupling equations is achieved under the finite difference framework, which can be solved by a nonlinear multigrid method. Numerical examples are carried out to verify the capability of the proposed modified model. Furthermore, we compare the results obtained by the original and modified model in detail to illustrate the significance of the modification.

The remainder of this paper is organized as follows. Section 2 introduces the original energy function of multiphase fluid flows and generates the modified energy function. Section 3 describes the numerical solution of the proposed multiphase model. Numerical examples are carried out in Section 4. Finally, concluding remarks are given in Section 5.

2. Methodology

2.1. The mixture of N-component immiscible fluids

The non-dimensional N-component system is obtained by coupling the CH equation with the Navier–Stokes(NS) equation as

$$\rho(\mathbf{c})\frac{\partial \mathbf{u}(\mathbf{x},t)}{\partial t} = -\rho(\mathbf{c})\mathbf{u}(\mathbf{x},t)\cdot\nabla\mathbf{u}(\mathbf{x},t) - \nabla p(\mathbf{x},t) + \frac{1}{Re}\nabla\cdot\left[\eta(\mathbf{c})\left(\nabla\mathbf{u}(\mathbf{x},t)+\nabla\mathbf{u}(\mathbf{x},t)^T\right)\right] + \mathbf{SF}, \tag{1a}$$

$$\nabla\cdot\mathbf{u}(\mathbf{x},t) = 0, \tag{1b}$$

$$\frac{\partial c_k(\mathbf{x},t)}{\partial t} + \mathbf{u}(\mathbf{x},t)\cdot\nabla c_k(\mathbf{x},t) = \frac{1}{Pe}\Delta\mu_k(\mathbf{x},t), \tag{1c}$$

$$\mu_k(\mathbf{x},t) = f(c_k) - \varepsilon^2\Delta c_k(\mathbf{x},t). \tag{1d}$$

Note that $\mathbf{c}(\mathbf{x},\ t) = (c_1, c_2, \ldots, c_N)$, $\mathbf{u}(\mathbf{x},\ t)$, $p(\mathbf{x},\ t)$, and $\mu_k(\mathbf{x},\ t)$ are the vector-value phase variable, velocity field, pressure field, and chemical potential of the phase k, respectively. The dimensionless parameters Re and Pe are the Reynolds number and Péclet number, respectively. Furthermore, $f(c_k) = \partial F/\partial c_k$ is the external force, where $F(\mathbf{c}) = \sum_{k=1}^{N}(1-c_k)^2 c_k^2/4$ is the fourth-order polynomial potential functional. We use ε to denote the finite thickness of the mathematically sharp interfaces between different phases. Note that $\rho(\mathbf{c}) = \sum_{k=1}^{N} c_k\rho_k$ and $\eta(\mathbf{c}) = \sum_{k=1}^{N} c_k\eta_k$ indicate the density and viscosity of multiphase incompressible fluid [24,28], respectively. In addition, we use **SF** to denote the surface tension force, which plays a key role in handling with multi-component system especially when the extreme topological changes happens to the interface [25,29]. Generally, the N-phase system has $N(N-1)/2$ possible interfaces. Considering the following two cases:

$$\begin{cases} Case\ \ 1: & N(N-1)/2 \le N, \quad N \le 3, \\ Case\ \ 2: & N(N-1)/2 > N, \quad N \ge 4. \end{cases} \tag{2}$$

For the first case, we illustrate with the example of three-phase flows. With respect to the given physical interface Γ_{kj} between phase $k(\Omega_k)$ and phase $j(\Omega_j)$, σ_{kj} denotes to be the surface tension coefficients and is decomposed into the specific surface tension coefficients σ_1, σ_2 and σ_3 as:

$$\sigma_{12} = \sigma_1 + \sigma_2, \quad \sigma_{23} = \sigma_2 + \sigma_3, \quad \sigma_{13} = \sigma_1 + \sigma_3, \tag{3}$$

which yields

$$\sigma_1 = (\sigma_{12} + \sigma_{13} - \sigma_{23})/2, \quad \sigma_2 = (\sigma_{12} + \sigma_{23} - \sigma_{13})/2, \quad \sigma_3 = (\sigma_{13} + \sigma_{23} - \sigma_{12})/2. \tag{4}$$

For the second case($N \ge 4$), we illustrate with the example of four-phase fluids. We should remark that the solution may not exist of the system generated by the decomposition [25]. However, we can possess a unique solution by applying some restrictions on the handling of surface tension. Here we limit the over-determined system under the guidance of least square idea. Note that we have no difficulty for solving the multi-phase system with over-determined issues. The physical surface tension coefficients σ_{kj} are defined as:

$$\sigma_{12} = \sigma_1 + \sigma_2, \quad \sigma_{23} = \sigma_2 + \sigma_3, \quad \sigma_{13} = \sigma_1 + \sigma_3, \quad \sigma_{14} = \sigma_1 + \sigma_4, \quad \sigma_{24} = \sigma_2 + \sigma_4, \quad \sigma_{34} = \sigma_3 + \sigma_4. \tag{5}$$

These four unknown σ_1, σ_2, σ_3 and σ_4 can be calculated by solving the linear system (5) with the least square method. Let us consider the over-determined problem, i.e. $A\sigma = Y$, where

$$A = \begin{bmatrix} 1 & 0 & 1 & 1 & 0 & 0 \\ 1 & 1 & 0 & 0 & 1 & 0 \\ 0 & 1 & 1 & 0 & 0 & 1 \\ 0 & 0 & 0 & 1 & 1 & 1 \end{bmatrix}^T, \quad \sigma = \begin{bmatrix} \sigma_1 & \sigma_2 & \sigma_3 & \sigma_4 \end{bmatrix}^T, \quad Y = \begin{bmatrix} \sigma_{12} & \sigma_{23} & \sigma_{13} & \sigma_{14} & \sigma_{24} & \sigma_{34} \end{bmatrix}^T. \tag{6}$$

By minimizing $\|A\sigma - Y\|^2$, we can obtain $\sigma = (A^TA)^{-1}A^TY$. Thus, the surface tension force of multi-component fluid system can be defined as

$$\mathbf{SF} := \sum_{k=1}^{N}\mathbf{SF}_k = \sum_{k=1}^{N}\sigma_k\kappa(c_k)\,\mathbf{N}(c_k)\,\delta(c_k), \tag{7}$$

where $\kappa(c_k) = \nabla\cdot(\nabla c_k/|\nabla c_k|)$ is the mean curvature, $\mathbf{n}(c_k) = (\nabla c_k/|\nabla c_k|)$ is the unit normal vector and $\delta(c_k) = |\nabla c_k|$ is the smoothed Dirac delta function of the kth fluid interface.

It is remarkable that the constraints on the model parameters limit the applicability of our theory and the construction of the multi-phase CH model does not satisfy the conditions of physical consistency with an increasing number of components. However, the proposed method with least squares procedure makes mathematical sense and is appropriate in this paper. For more investigation of free-energy functional or the diffusion equations of the multicomponent system, Tóth and his collaborators provided series physically deep Refs. [30,31], which compensated for the lack of mathematical and physical consistency in the multicomponent model. Based on their framework, the free energy density landscape has no multicomponent local minima, which prevents the system from falling into a multicomponent homogeneous state during spinodal decomposition. To demonstrate the physical consistency of the hydrodynamic system, they derived dynamic equations describing the time evolution of an isothermal multicomponent liquid mixture with the compact mathematical formulation, which can be applied for many liquid systems of practical importance featuring variable density. More multiphase-field theories can be found in [32,33]. Although the classical physical property such as mass conservation can be satisfied by the original CH model, the following issues cannot be consoled: (i) Non-physical motion influenced by the model. (ii) Sharpened interface without hyperbolic tangent property. (iii) The enclosed area by the interfaces is not preserved. In order to solve the problems mentioned above, we modified the original model in the next subsection.

2.2. The modification of the N-component Canh–Hilliard Equation

For N-component system with incompressible property [28], we have

$$c_1 + c_2 + \cdots + c_k + \cdots + c_N = 1, \tag{8}$$

where c_k represents the volume fraction of kth fluid and N is the number of phases. The original N-component CH equation Eqs. (1c) and (1d) can be derived from the Helmholtz free energy functional:

$$\mathscr{E}_{CH} = \sum_{k=1}^{N} \mathscr{E}_i = \sum_{k=1}^{N} \int_{\Omega} \left(F(c_k) + \frac{\varepsilon^2}{2} |\nabla c_k|^2 \right) d\mathbf{x}. \tag{9}$$

The original CH equation derived by a 'gradient flow' as [34]:

$$(c_k)_t = M\Delta \frac{\delta \mathscr{E}_k}{\delta c_k}, \tag{10}$$

where $\mu_k = \delta \mathscr{E}_k / \delta c_k$ is the chemical potential of phase k and can be derived from the energy functional Eq. (9) as:

$$\begin{aligned} \frac{d}{d\xi} \mathscr{E}_k(c_k + \xi\psi)\Big|_{\xi=0} &= \int_{\Omega} \left(\psi F'(c_k) + \varepsilon^2 \nabla\psi \cdot \nabla c_k \right) d\mathbf{x} \\ &= \int_{\Omega} \left(F'(c_k) - \varepsilon^2 \Delta c_k \right) \psi d\mathbf{x} + \int_{\partial\Omega} \varepsilon^2 \frac{\partial c_k}{\partial n} \psi ds \\ &= \int_{\Omega} \left(F'(c_k) - \varepsilon^2 \Delta c_k \right) \psi d\mathbf{x}. \end{aligned} \tag{11}$$

Here $\int_{\Omega} \psi d\mathbf{x} = 0$ and $\partial c_k / \partial n = 0$ at $\partial\Omega$. Thus, the chemical potential of the N-component system can be obtained by

$$\mu_k = \frac{\delta \mathscr{E}_{\mathrm{CH}}}{\delta c_k} = F'(c_k) - \varepsilon^2 \Delta c_k. \tag{12}$$

To keep Eq. (8), the modified term $\beta(\mathbf{c})$ has been added to the chemical potential such that

$$\mu_k(\mathbf{x}, t) = F'(c_k(\mathbf{x}, t)) - \varepsilon^2 \Delta c_k(\mathbf{x}, t) + \beta(\mathbf{c}) c_k, \tag{13}$$

where $\beta(\mathbf{c}) = -\sum_{k=1}^{N} F'(c_k)$, which can be derived from

$$\begin{aligned} 0 &= \frac{\partial (\sum_{k=1}^{N} c_k)}{\partial t} = \sum_{k=1}^{N} \frac{\partial c_k}{\partial t} = M\Delta \sum_{k=1}^{N} \mu_k \\ &= M\Delta \sum_{k=1}^{N} \left(F'(c_k) - \varepsilon^2 \Delta c_k + \beta(\mathbf{c}) c_k \right) \\ &= M\Delta \left(\sum_{k=1}^{N} F'(c_k) + \sum_{k=1}^{N} \beta(\mathbf{c}) c_k \right), \end{aligned}$$

After that the N-component CH model can be described as

$$\begin{cases} \dfrac{\partial c_k}{\partial t}(\mathbf{x}, t) = M\Delta \mu_k(\mathbf{x}, t), \mathbf{x} \in \Omega, 0 < t \le T, \\ \mu_k(\mathbf{x}, t) = F'(c_k(\mathbf{x}, t)) - \varepsilon^2 \Delta c_k(\mathbf{x}, t) - \beta(\mathbf{c}) c_k, \\ \dfrac{\partial \mu_k(\mathbf{x}, t)}{\partial \mathbf{n}} = 0, \mathbf{x} \in \partial\Omega. \end{cases} \tag{14}$$

To satisfy hyperbolic tangent properties [35], a penalty term has been added into Eq. (14) and obtain the modified N-component CH system as:

$$\begin{cases} \dfrac{\partial c_k}{\partial t}(\mathbf{x}, t) = \dfrac{1}{Pe} \Delta \mu_k \\ \quad + \lambda \dfrac{1}{Pe} \left(\Delta c_k - \dfrac{1}{\sqrt{2}\varepsilon} \nabla \cdot \left((1 - c_k) c_k \dfrac{\nabla c_k}{|\nabla c_k|} \right) \right), \ \mathbf{x} \in \Omega, 0 < t \le T, \\ \mu_k(\mathbf{x}, t) = F'(c_k) - \varepsilon^2 \Delta c_k + \beta(\mathbf{c}) c_k, \\ \dfrac{\partial \mu_k(\mathbf{x}, t)}{\partial \mathbf{n}} = 0, \mathbf{x} \in \partial\Omega. \end{cases}$$

Therefore, the modified phase-field model under hydrodynamic framework can be rewritten as

$$\begin{cases} \rho(\mathbf{c}) \dfrac{\partial \mathbf{u}(\mathbf{x}, t)}{\partial t} = -\rho(\mathbf{c}) \mathbf{u}(\mathbf{x}, t) \cdot \nabla \mathbf{u}(\mathbf{x}, t) \\ \quad - \nabla p(\mathbf{x}, t) + \dfrac{1}{Re} \nabla \cdot \left[\eta(\mathbf{c}) \left(\nabla \mathbf{u}(\mathbf{x}, t) + \nabla \mathbf{u}(\mathbf{x}, t)^T \right) \right] + \mathbf{SF}, \\ \nabla \cdot \mathbf{u}(\mathbf{x}, t) = 0, \\ \dfrac{\partial c_k(\mathbf{x}, t)}{\partial t} + \mathbf{u}(\mathbf{x}, t) \cdot \nabla c_k = \dfrac{1}{Pe} \Delta \mu_k(\mathbf{x}, t) \\ \quad + \dfrac{\lambda}{Pe} \left(\Delta c_k - \dfrac{1}{\sqrt{2}\varepsilon} \nabla \cdot \left((1 - c_k) c_k \dfrac{\nabla c_k}{|\nabla c_k|} \right) \right), \\ \mu_k(\mathbf{x}, t) = f(c_k) - \varepsilon^2 \Delta c_k - \beta(\mathbf{c}) c_k. \end{cases} \tag{15}$$

3. Numerical solution

Let us define $N_x \times N_y$ as the number of cells in the computational domain, where N_x and N_y are even integers. Let h be the uniform mesh size and the center of each cell Ω_{ij} can be denoted as $(x_i, y_j) := \left((i - \frac{1}{2})h, (j - \frac{1}{2})h \right)$ for $i = 1, \ldots, N_x$ and $j = 1, \ldots, N_j$. Therefore, vertices of cells can be denoted as $(x_{i+\frac{1}{2}}, y_{j+\frac{1}{2}}) := (ih, jh)$. Let c_k^n denote the approximation of the concentration of the kth component at time $n\Delta t$, where $\Delta t = T/N_t$ is the temporal step, T is the total computational time and N_t is the total number of computational time steps. We use a staggered marker-and-cell (MAC) mesh [36], which contains the pressure field and phase-field at the center of cells and the velocity fields at cell interfaces. The updated $\mathbf{u}^{n+1}$, $\mathbf{c}^{n+1}$ and p^{n+1} in each step can be solved by the calculated value $\mathbf{u}^n$ and $\mathbf{c}^n$:

$$\begin{aligned} &\rho(\mathbf{c}^n) \frac{\mathbf{u}^{n+1} - \mathbf{u}^n}{\Delta t} + \rho(\mathbf{c}^n) \mathbf{u}^n \cdot \nabla_d \mathbf{u}^n \\ &\quad = -\nabla_d p^{n+1} + \frac{1}{Re} \nabla_d \cdot \eta(\mathbf{c}^n) \left[\nabla_d \mathbf{u}^n + \left(\nabla_d \mathbf{u}^n \right)^T \right] + \mathbf{SF}^n, \end{aligned} \tag{16a}$$

$$\nabla_d \cdot \mathbf{u}^{n+1} = 0, \tag{16b}$$

$$\begin{aligned} &\frac{c_k^{n+1} - c_k^n}{\Delta t} + \left(\mathbf{u}^{n+1} \cdot \nabla_d c_k^n \right) \\ &\quad = \frac{1}{Pe} \Delta_d \mu_k^{n+1} + \frac{\lambda}{Pe} \left(\Delta_d c_k^n - \frac{1}{\sqrt{2}\varepsilon} \nabla_d \cdot \left((1 - c_k^n) c_k^n \frac{\nabla_d c_k^n}{|\nabla_d c_k^n|} \right) \right), \end{aligned} \tag{16c}$$

$$\mu_k^{n+1} = f(c_k^{n+1}) + \frac{c_k^{n+1}}{4} - \frac{c_k^n}{4} - \varepsilon^2 \Delta_d c_k^{n+1} + \beta(c_k^n) c_k^n. \tag{16d}$$

Here, ∇_d and $\nabla_d \cdot$ are the discrete gradient and divergence operators, respectively. The projection method [37–40] is performed to handle the incompressible NS equation as follows:

Step1. Initialization of the phase-field $\mathbf{c}^0$, velocity field $\mathbf{u}^0$, the surface tension force $\mathbf{SF}^0$, density ρ^0 and viscosity η^0.

Step2. Formulation based on the NS functional Eqs. (16a) and (16b). The intermediate velocity field $\mathbf{u}^*$ can be solved as

$$\begin{aligned} &\rho(\mathbf{c}^n) \frac{\mathbf{u}^* - \mathbf{u}^n}{\Delta t} + \rho(\mathbf{c}^n) \mathbf{u}^n \cdot \nabla_d \mathbf{u}^n = \\ &\quad \frac{1}{Re} \nabla_d \cdot \eta(\mathbf{c}^n) \left[\nabla_d \mathbf{u}^n + \left(\nabla_d \mathbf{u}^n \right)^T \right] + \mathbf{SF}^n, \end{aligned} \tag{17}$$

where the convection term $\mathbf{u}^n \cdot \nabla_d \mathbf{u}^n$ can be solved by a ENO procedure proposed in Ref. [41]. Considering the following equation

$$\frac{\mathbf{u}^{n+1} - \mathbf{u}^*}{\Delta t} = -\frac{1}{\rho(\mathbf{c}^n)} \nabla_d p^{n+1}, \tag{18}$$

where the velocity field $\mathbf{u}^{n+1}$ satisfies $\nabla_d \cdot \mathbf{u}^{n+1} = 0$. Applied the divergence operator to Eq. (18), the pressure of $(n+1)$ time step

can be obtained as

$$\nabla_d \cdot \left(\frac{1}{\rho(\mathbf{c}^n)} \nabla_d p^{n+1} \right) = \frac{1}{\Delta t} \nabla_d \cdot \mathbf{u}^*. \tag{19}$$

Here we use a multigrid method for the computation of pressure p^{n+1} in this Poisson equation as

$$\nabla_d \cdot \left(\frac{1}{\rho^n} \nabla_d p_{ij}^{n+1} \right) = \left(\frac{p_{i+1,j}^{n+1}}{\rho^n_{i+\frac{1}{2},j}} + \frac{p_{i-1,j}^{n+1}}{\rho^n_{i-\frac{1}{2},j}} + \frac{p_{i,j+1}^{n+1}}{\rho^n_{i,j+\frac{1}{2}}} + \frac{p_{i,j-1}^{n+1}}{\rho^n_{i,j-\frac{1}{2}}} - \left(\frac{1}{\rho^n_{i+\frac{1}{2},j}} + \frac{1}{\rho^n_{i-\frac{1}{2},j}} + \frac{1}{\rho^n_{i,j+\frac{1}{2}}} + \frac{1}{\rho^n_{i,j-\frac{1}{2}}} \right) p_{ij}^{n+1} \right) / h^2.$$

Therefore, the velocity field can be updated as $\mathbf{u}^{n+1} = \mathbf{u}^* - \Delta t \nabla_d p^{n+1} / \rho(\mathbf{c}^n)$.

Step3. Formulation based on the CH functional Eqs. (16c) and (16d). With the known $\mathbf{c}^n$ and $\mathbf{u}^{n+1}$, we compute the phase-field $\mathbf{c}^{n+1}$ by a nonlinear full approximation storage multi-grid method at the implicit time level. The second-order central difference scheme is used for discretization of Eqs. (16c) and (16d). For more details of solving the nonlinear system with the multi-grid method, please refer to [42,43].

4. Experimental tests

In this section, various numerical experiments such as the evolution of triple junction with the prescribed contact angle, shape relaxation under multi-component liquid background, a convergence test with a rotate disk, deformation under shear flow, the simulation of falling droplet and the simulation of Kelvin–Helmholtz instability with ternary fluids, have been performed to demonstrate the efficiency of the proposed method. Unless otherwise specified, we will choose the computational domain as $\Omega = [0,\ 1] \times [0,\ 1]$ with a 256×256 mesh gird and use the following parameters in the numerical simulations: $\lambda = 0.1$, $Re = 200$, $\varepsilon = 5h/(4\sqrt{2}\text{atanh}(0.9))$, $Pe = 1/\varepsilon$, and $\Delta t = 5h^2$.

4.1. Triple junction with a prescribed contact angle

In this section, we investigate the equilibrium phase interface with a prescribed contact angle, which is denoted as θ. Since the original CH model does not conserve the volume, there will be a loss of accuracy during the computation. Denoting the two-dimension velocity field as $\mathbf{v} := (u,\ v)$. The initial conditions are chosen as

$$\begin{cases} u(x,y,0) = v(x,y,0) = 0,\ \ p(x,y,0) = 0, \\ c_1(x,y,0) = 0.5 + 0.5 \tanh\left((|x-0.25| + |x-0.55| + |y-0.50| + |y-0.80| - 0.6)/(2\sqrt{2}\varepsilon) \right), \\ c_2(x,y,0) = 0.5 + 0.5 \tanh\left((|x-0.25| + |x-0.55| + |y-0.50| + |y-0.20| - 0.6)/(2\sqrt{2}\varepsilon) \right), \\ c_3(x,y,0) = 0.5 + 0.5 \tanh\left((|x-0.55| + |x-0.85| + |y-0.35| + |y-0.65| - 0.6)/(2\sqrt{2}\varepsilon) \right), \\ c_4(x,y,0) = 1 - c_1(x,y,0) - c_2(x,y,0) - c_3(x,y,0). \end{cases} \tag{20}$$

Let us denote θ_1, θ_2 and θ_3 as the interfacial angles of phase 1(red region), phase 2(blue region) and phase 3(green region), respectively. The interfacial angles reflect the equilibrium of surface tensions between different phases, i.e. $\theta_1 + \theta_2 + \theta_3 = 2\pi$ and $sin(\theta_1)/\sigma_{23} = sin(\theta_2)/\sigma_{13} = sin(\theta_3)/\sigma_{12}$, where σ_{ij} is the surface tension between phase k and phase j. The numerical simulation is performed until $\|c_k^{n+1} - c_k^n\|_2 / \|c_k^n\|_2 \le 1e-6$. Fig. 1 demonstrates the evolution of ternary immiscible liquids in another liquid from an initially rectangular state to an equilibrium state. Here we use $\sigma_1 = \sigma_2 = \sigma_3 = 1$, which causes the interfacial angles to satisfy $\theta_1 = \theta_2 = \theta_3 = 2\pi/3$ at the equilibrium state. The numerical simulations show that the results by the proposed scheme are consistent with the theoretical results. Meanwhile, the proposed model can capture the interface deformation well and conserve the enclosed area of multiple phases by comparing with the original CH model. In Fig. 1(c), we plot the 0.5 level contour line at the indicated time $t = 1.5$. The solid lines show the results of the modified CH model and the dash lines show the results of the original CH model. It is obvious that the results obtained by the modified model significantly reduce the enclosed area loss.

4.2. Coalescence of two kissing bubbles under ternary liquid background

In this section, the simulation of shape relaxation by two kissing circles under ternary liquids background has been demonstrated. The initial conditions are chosen as

$$\begin{cases} u(x,y,0) = v(x,y,0) = 0,\ \ p(x,y,0) = 0, \\ c_1(x,y,0) = 0.5 + 0.5 \tanh\left((0.2 - \sqrt{|x-0.5|^2 + (y-0.5)^2})/(2\sqrt{2}\varepsilon) \right), \\ c_2(x,y,0) = 0.5 - 0.5 \tanh\left((1-c_1)(x-0.3)/(2\sqrt{2}\varepsilon) \right), \\ c_3(x,y,0) = 0.5 + 0.5 \tanh\left((1-c_1)(x-0.7)/(2\sqrt{2}\varepsilon) \right), \\ c_4(x,y,0) = 1 - c_1(x,y,0) - c_2(x,y,0) - c_3(x,y,0). \end{cases} \tag{21}$$

As can be seen from Fig. 2, the merging deformation of two circles next to each other has appeared under the influence of surface tension. By comparing the results of Fig. 2(a) and (b) at different indicated time, we can see that the proposed model can conserve the enclosed area under the premise of keeping the original mechanism. In order to further study the volume conservation of multi-component liquid, we define the polygonal area $A(\phi)$ as

$$A(\phi) := \sum_{i=0}^{s-1} (x_i y_{i+1} - y_i x_{i+1}) / 2 \tag{22}$$

which is surrounded by $p_i(x,y)(i = 0, 1, \ldots, s-1)$ as shown in Fig. 3(a). In Fig. 3(b), the comparison of the normalized polygonal areas between the modified CH model and the original CH model has been demonstrated. From these results, it is obvious that the modified model is indeed volume conservative, while the area obtained by the original model decreases.

4.3. Convergence test

To investigate the convergence rates with respect to space, we demonstrate various tests with increasingly finer grids $h = 1/2^n (n = 6,\ 7,\ 8)$ in the computational domain $\Omega = [0,\ 1] \times [0,\ 1]$. We use the following initial conditions:

$$\begin{cases} u(x,y,0) = 20(y-0.5),\ \ v(x,y,0) = -20(x-0.5), \\ p(x,y,0) = 0, \\ c_1(x,y,0) = 0.5 + 0.5 \tanh\left((0.1 - \sqrt{(x-0.25)^2 + (y-0.5)^2})/(2\sqrt{2}\varepsilon) \right), \\ c_2(x,y,0) = 0.5 + 0.5 \tanh\left((0.2 - \sqrt{(x-0.75)^2 + (y-0.5)^2})/(2\sqrt{2}\varepsilon) \right), \\ c_3(x,y,0) = 1 - c_1(x,y,0) - c_2(x,y,0). \end{cases}$$

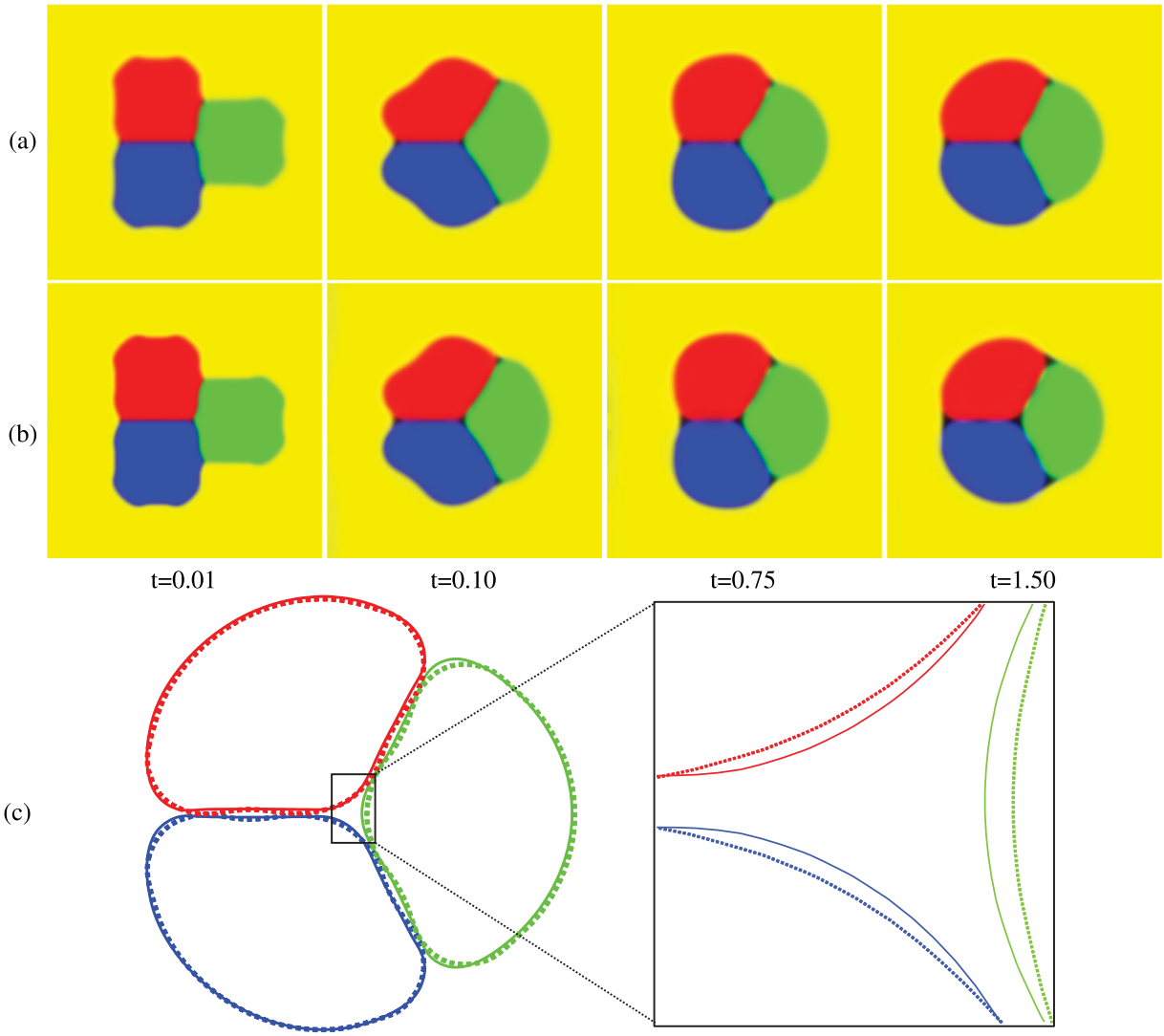

Fig. 1. The dynamical behaviors of multi-component liquid with a prescribed contact angle. (a) is the simulation by the modified CH model. (b) is the simulation by the original CH model. From left to right, the indicated time is $t = 0.01$, 0.10, 0.75, and 1.50, respectively. (c) is the interface profiles of the ternary liquid and its close-up view. The solid lines show the results of the modified CH model and the dash lines show the results of the original CH model. (For interpretation of the references to color in this figure legend, the reader is referred to the web version of this article.)

(23)

where the background velocity field does not change corresponds to time, i.e., $u(x, y, t) = u(x, y, 0)$ and $v(x, y, t) = v(x, y, 0)$. It has to be remarked that the two circles should not change the shapes during the rotation. The results of different mesh grids with the modified CH model at indicated time $t = 0$, $\pi/40$, $\pi/20$, $3\pi/40$, and $\pi/10$ are presented in Fig. 4. Fig. 4(a) is the evolution of the rotate disk under a coincided velocity background fluids with the modified CH model. Fig. 4(b) shows numerical results with refined spatial grids and its close-up view. Here we use the red line, green line and the blue line to represent the results obtained by the 128×128, 256×256, and 512×512 mesh grids, respectively. The exact solution is marked as black circle. From these results, we can see that the convergence under spatial refinements is evident. Let us define the error and convergence rate as:

$$\begin{cases} e_{hij} = \phi^t_{hij} - \phi^0_{hij}, \\ r_h = log_2 \left(\|e_h\|_2 / \|e_{h/2}\|_2 \right), \end{cases} \tag{24}$$

where $(\cdot)^t_{hij}$ represents the value of the point (i, j) at the indicated time t with spatial step h and $\|\cdot\|$ is the l_2-norm. We run this procedure until $t = 2\pi/5$ and present the errors and convergent rates in Table 1. These results suggest that the proposed method is of second-order spatial accuracy and first-order temporal accuracy as expected from the discretization. By comparing the results of the two models, we can see that our proposed model obtains more accurate results.

Table 1
Error and convergence rate of the proposed schemes with various mesh grids. The temporal step size is fixed as $\Delta t = 5h^2$.

Mesh grid sizes	128×128		256×256		512×512
Original CH model: l_2 error	1.912e−4		4.446e−5		1.040e−5
Rate		2.10		2.10	
Modified CH model: l_2 error	1.615e−4		3.916e−5		9.982e−6
Rate		2.04		1.97	

4.4. Droplet deformation under shear flow background

We demonstrate the deformation of a suspended droplet under the influence of shear flow in this section. Fig. 6 (a–c) shows the temporal evolution of the droplet deformation with the initial

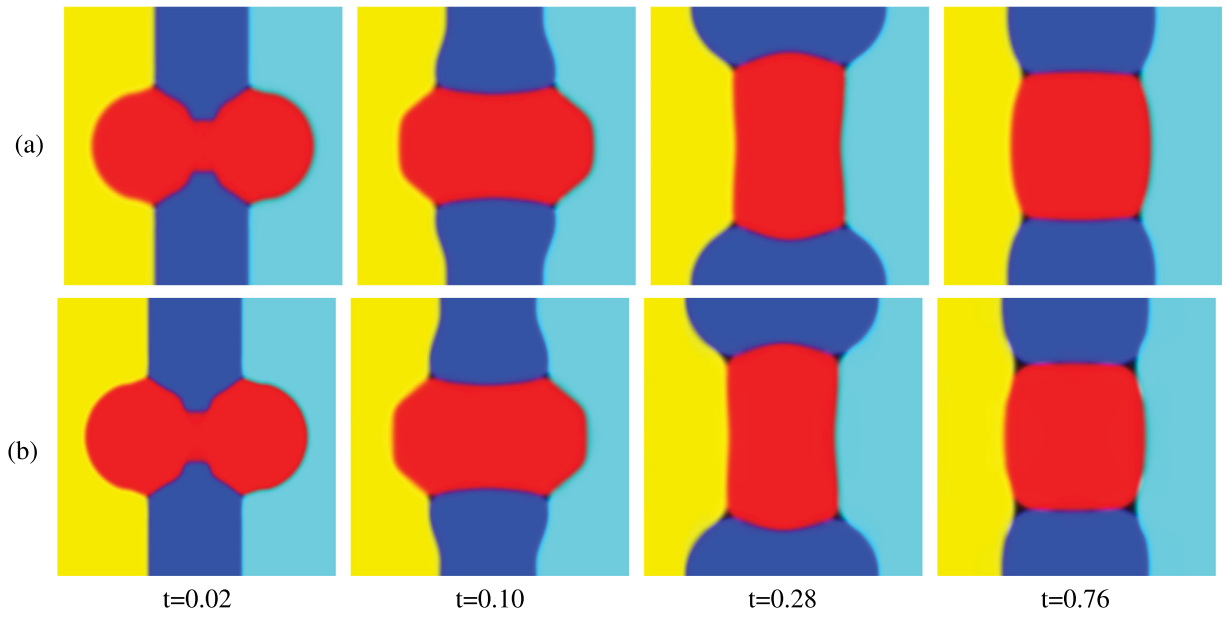

Fig. 2. The dynamical behaviors of the two kissing circles in triple phase liquids. (a) is the results by the modified CH model. (b) is the results by the original modified CH model. From left to right, the indicated time is $t = 0.02$, 0.10, 0.28, and 0.76.

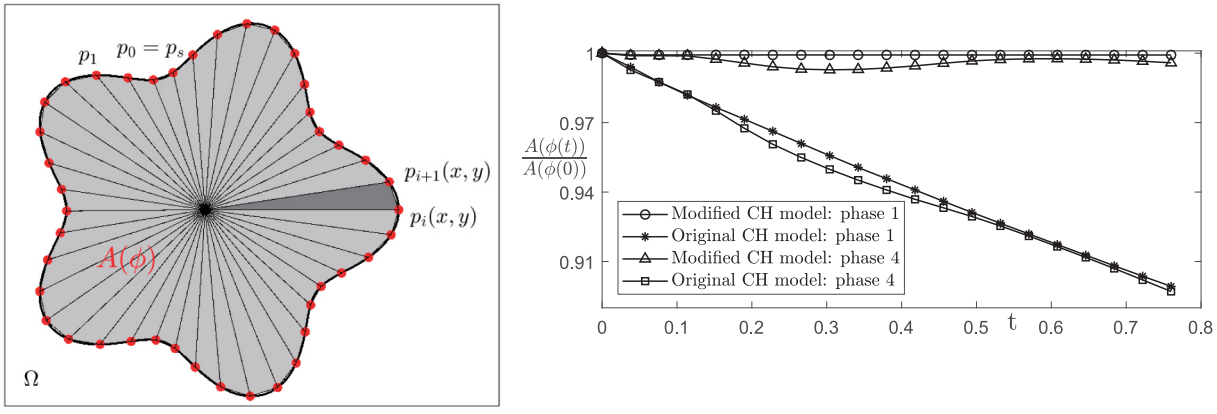

Fig. 3. (a) Numerical polygonal area $A(\phi)$ bounded by points $p_i(x, y)(i = 0, 1, \ldots, s-1)$, which are located on the 0.5 level of the phase-field and $A(\phi) = \sum_{i=0}^{s-1}(x_i y_{i+1} - y_i x_{i+1})/2$. (b) Time evolution of the normalized polygonal areas for the simulations of Fig. 2.

conditions as shown in Fig. 5 (a–c), respectively. For the sake of clarification, we denote the radius of the small droplet as r and the radius of the big droplet as R. As shown in Fig. 5(a), the big droplet of radius $R = 0.2$ and the small droplet of radius $r = 0.15$ are positioned at the center of Ω. Due to the surface tension, fracture appears in Fig. 6(a). As shown in Fig. 5(b), the big droplet of radius $R = 0.2$ and the small droplet of radius $r = 0.1$ are positioned at the center of Ω. It is obvious that the two droplets deform in the same direction and then in the opposite direction, gradually stabilize to the initial state. Therefore, the size difference between the two droplets affects the surface tension of the interface profile. When the droplet size is small, the surface tension becomes larger. In order to demonstrate the impact of the velocity field, we increase the value of background velocity in the computational domain, which has been shown in Fig. 6(c). By comparing the deformation of the same composite droplet in different velocity fields, we can see that the increase of kinetic energy causes the droplet to break through the surface tension constraint. However, the composite droplet finally changes into an ellipse shape under the influence of surface tension, which corresponds with the physical context.

4.5. Simulation of the falling droplet with two different density ratios

To demonstrate the performance of our modified CH functional in interface capturing, we consider the falling droplet deformation with high density ratios in two-dimensional space. The drop with radius $r = 0.1$ is positioned at $(0.25,\ 0.75)$ in the computational domain $\Omega = [0,\ 0.5] \times [0,\ 1]$ with a 128×256 mesh grid. Here we use $h = 1/256$ and $dt = 5h^2$. For the sake of clarification, we mark the domain with black, red and white color as phase 1, phase 2 and phase 3, respectively. The different densities of the three phases are denoted as ρ_1, ρ_2 and ρ_3. Let us add a buoyancy term to the NS equation as

$$\rho(\mathbf{c}^n)\frac{\mathbf{u}^{n+1} - \mathbf{u}^n}{\Delta t} + \rho(\mathbf{c}^n)(\mathbf{u} \cdot \nabla_d \mathbf{u})^n = -\nabla_d p^{n+1} + \frac{1}{Re}\nabla_d \cdot \eta(\mathbf{c}^n)\left[\nabla_d \mathbf{u}^n + (\nabla_d \mathbf{u}^n)^T\right] + \mathbf{SF}^n + \frac{\rho(\mathbf{c}) - \rho_1}{Fr}\mathbf{g}, \quad (25)$$

where Fr is the Froude number and equals 1 in this section. We denote $\mathbf{g} := (0,\ -1)$ as the gravity acceleration and choose the

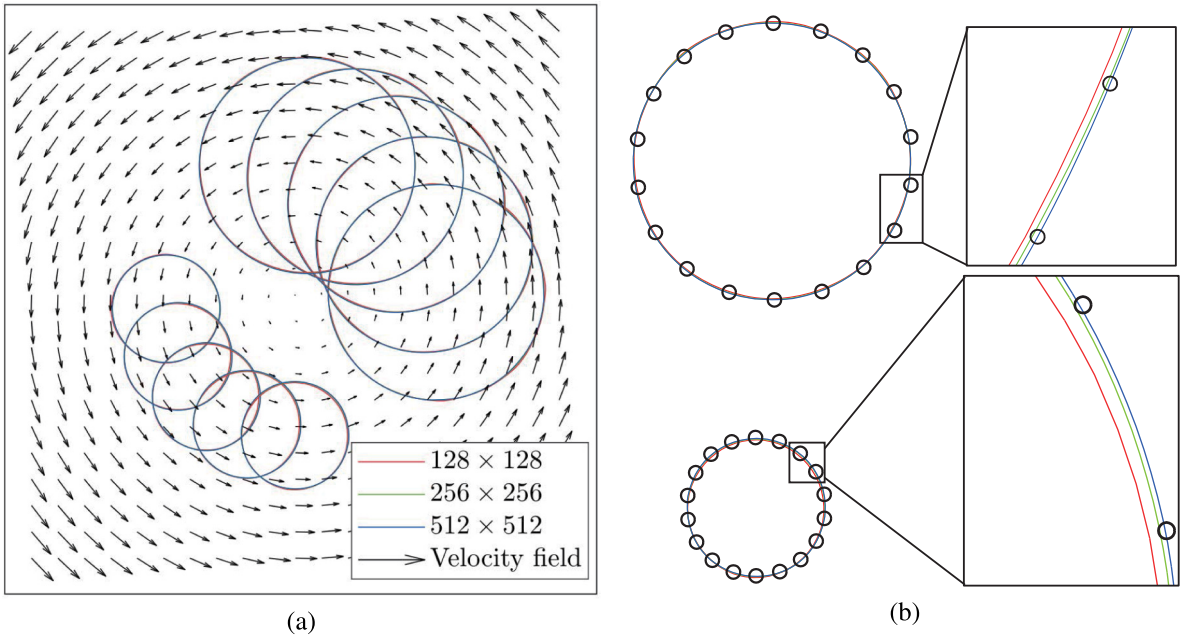

Fig. 4. (a) Temporal evolution of the rotate disk under a coincided velocity background fluids flows by the modified CH model. (b) Convergence tests with refined spatial grids and the close-up view. The red line, green line and the blue line represent the results obtained by the 128 × 128, 256 × 256 and 512 × 512 mesh, respectively. The exact solution is marked as the black circle. (For interpretation of the references to color in this figure legend, the reader is referred to the web version of this article.)

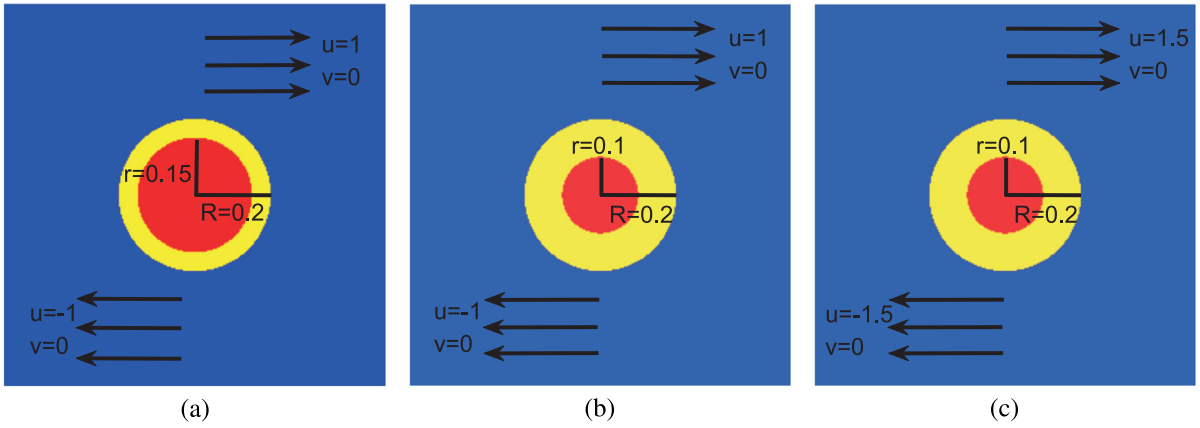

Fig. 5. Schematic illustration of the initial conditions. (a) $R = 0.2$ and $r = 0.15$. (b) $R = 0.2$ and $r = 0.1$. (c) $R = 0.2$ and $r = 0.1$.

initial conditions as

$$\begin{cases} u(x,y,0) = v(x,y,0) = 0, \;\; p(x,y,0) = 0, \\ c_1(x,y,0) = 0.5 \\ \quad + 0.5\tanh\left((0.1 - \sqrt{(x-0.25)^2 + (y-0.75)^2})/(2\sqrt{2}\varepsilon)\right), \\ c_3(x,y,0) = 0.5 + 0.5\tanh\left((0.5-y)/(2\sqrt{2}\varepsilon)\right), \\ c_2(x,y,0) = 1 - c_1(x,y,z,0) - c_3(x,y,z,0). \end{cases} \tag{26}$$

We simulate the falling droplet phenomenon under two different density ratio background. In Fig. 7, the density ratio is set as $\rho_1 : \rho_2 : \rho_3 = 1 : 10 : 10$. The results of the modified CH functional and original CH functional are demonstrated in Fig. 7(a) and (b), respectively. Since ϕ_2 and ϕ_3 have the same density, the droplet will not pass through the interface and stay at the middle between phase 1 and phase 2 eventually. We can see that a few liquid of phase 1 is squeezed between phase 2 and phase 3 due to the viscosity and surface tension. Observing the evolution, the captured interface of the falling droplet is constantly following the hyperbolic tangent constraints by the modified CH model. As shown in Fig. 8, the density ratio is $\rho_1 : \rho_2 : \rho_3 = 1 : 1 : 10$. We present the results of the modified CH functional in Fig. 8(a) and the results of the original CH functional in Fig. 8(b). From left to right, the indicated times are $t = 0$, 0.2, 0.4, 0.8, 1.0, 1.2, 1.4, and 1.6, respectively. As can be seen, the shape of droplet is changed because of the joint influence of velocity field and surface tension

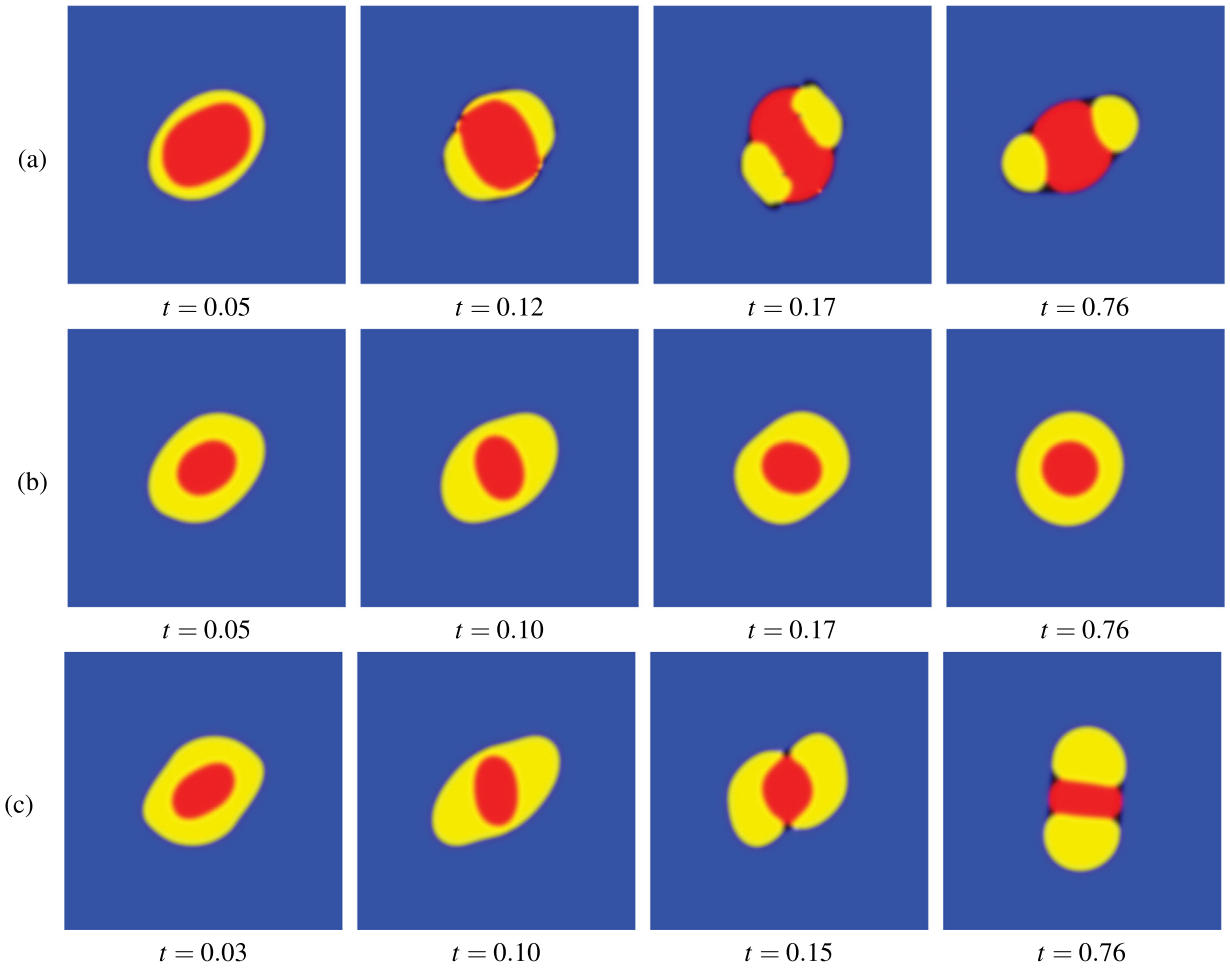

Fig. 6. The dynamical behaviors of the composite droplet under shear flow background liquid until the indicated time $t = 0.76$. The initial conditions of (a), (b) and (c) correspond to Fig. 5(a)–(c), respectively.

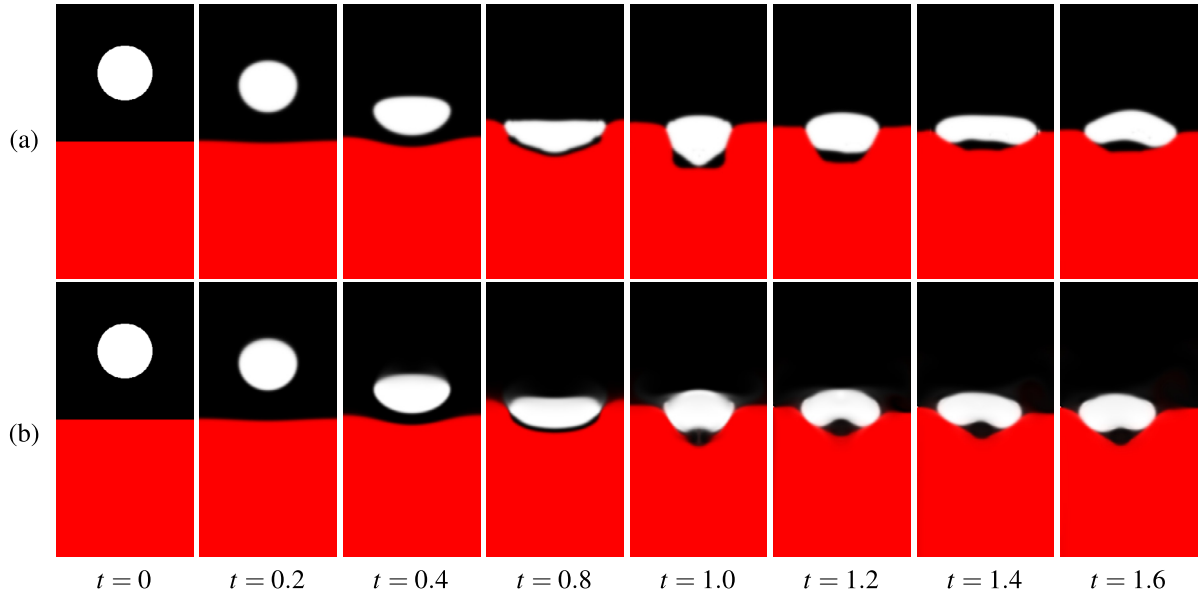

Fig. 7. The dynamical behaviors of the falling droplet between the two stratified fluids. The color in black (upper half), red (lower half) and white (falling drop) represent phase 1, 2 and 3, respectively. The density ratio is $\rho_1 : \rho_2 : \rho_3 = 1 : 10 : 10$. (a) is the results of the modified CH model. (b) is the results of the original CH model. (For interpretation of the references to color in this figure legend, the reader is referred to the web version of this article.)

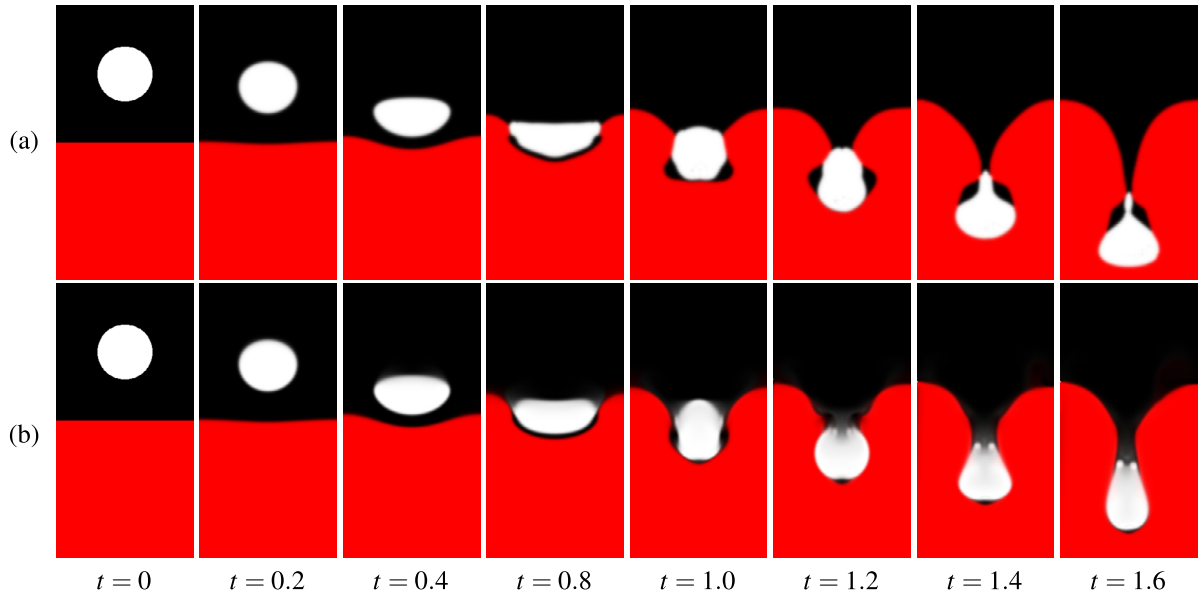

Fig. 8. The dynamical behaviors of the falling droplet between the two stratified fluids. The color in black (upper half), red (lower half) and white (falling droplet) represent phase 1, 2 and 3, respectively. The density ratio is $\rho_1 : \rho_2 : \rho_3 = 1 : 1 : 10$. From left to right, the indicated times are $t = 0, 0.2, 0.4, 0.8, 1.0, 1.2, 1.4$ and 1.6, respectively. (a) is the results of the modified CH model. (b) is the results of the original CH model. (For interpretation of the references to color in this figure legend, the reader is referred to the web version of this article.)

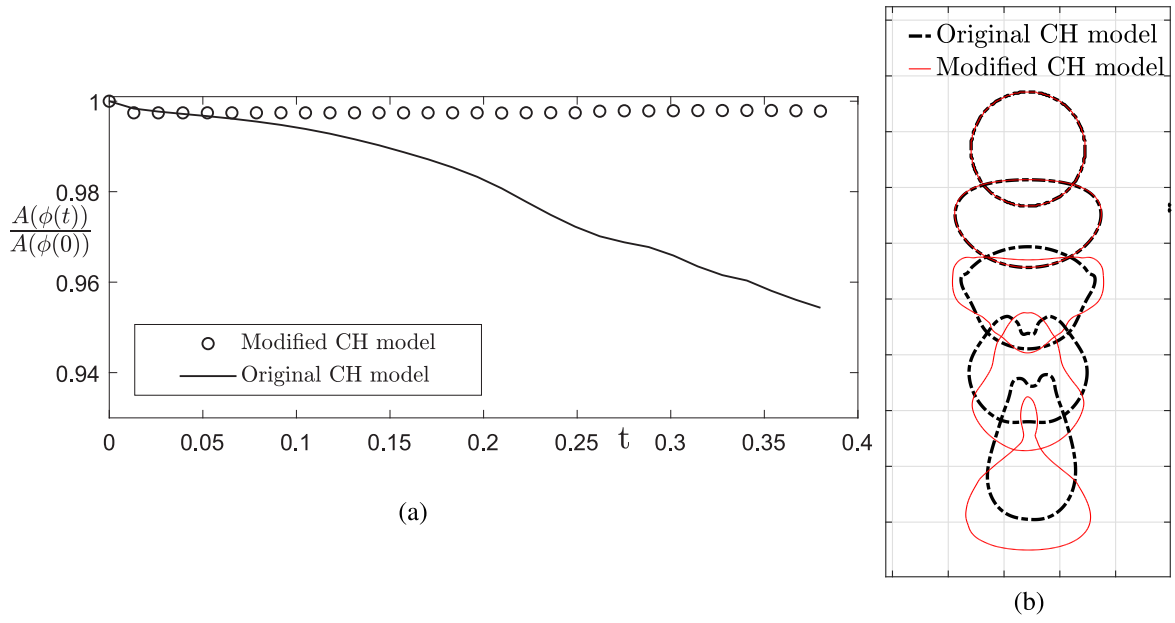

Fig. 9. Comparison between the modified CH model and the original CH model with falling droplets. (a) Temporal evolution of the normalized polygonal areas. (b) Temporal evolution of the location of falling droplets.

when it passes through the interface between phase 1 and phase 2. The falling droplet continues to stretch the thread until a pinch off of the main droplet occurs eventually due to the Rayleigh–Taylor instability [44]. Comparing the results in Fig. 8(a) and (b), better results in preserving the area can be obtained by using the modified model. We present the line chart of the polygonal areas of the two models in Fig. 9(a). As can be seen that the proposed model reduces the polygonal area loss significantly, while the original CH model does not preserve the area. In Fig. 9(b), we perform the droplet trajectories by the two models in the same frame and plot the 0.5-contour line at $t = 0, 0.4, 0.8, 1.2$, and 1.6, respectively. The shapes and locations of the two droplet has changed with respect to time due to the different surface tension.

4.6. Demonstration of Kelvin–Helmholtz instability with ternary fluids

The Kelvin–Helmholtz(KH) instability occurs between two fluids when there is a sufficiently large velocity difference [45]. By applying a small amplitude perturbed interface between the ternary fluids, the comparison results of the two models has been demonstrated in Fig. 10. We plot the 0.5-level contour line to represent the interface profiles between the ternary liquids. The

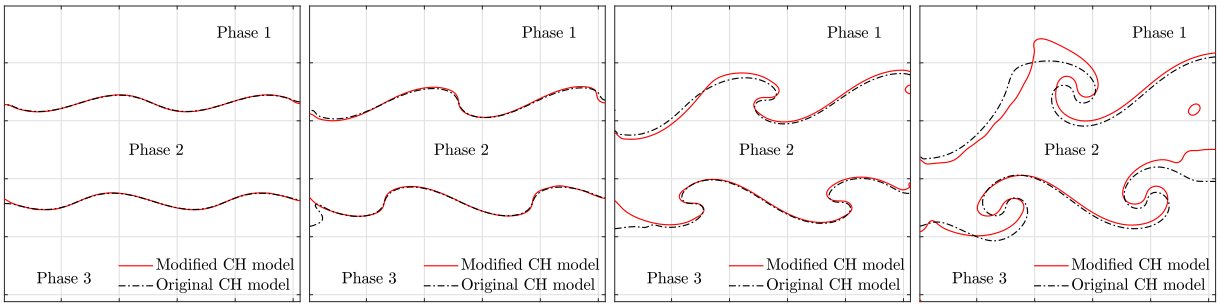

(a) $t = 0.1$ (b) $t = 0.2$ (c) $t = 0.3$ (d) $t = 0.45$

Fig. 10. Comparison of the phase-field with sinusoidal interface perturbations between the modified CH model and the original CH model. The red solid lines and black dash lines are the results obtained by the modified CH model and the original CH model, respectively. (For interpretation of the references to color in this figure legend, the reader is referred to the web version of this article.)

red solid lines represent the results with the modified CH model and the black dash lines represent the results with the original CH model. The initial conditions are considered as

$$\begin{cases} u(x,y,0) = 1 + \tanh\left((y - 0.66 - 0.02\sin(4\pi x))/(0.02\sqrt{2})\right) \\ \quad - \tanh\left((y - 0.33 - 0.02\sin(4\pi x))/(0.02\sqrt{2})\right), \\ v(x,y,0) = 0, \;\; p(x,y,0) = 0, \\ c_1(x,y,0) = 0.5 \\ \quad + 0.5\tanh\left((y - 2/3 - 0.01\sin(4\pi x))/(2\sqrt{2}\varepsilon)\right), \\ c_2(x,y,0) = 0.5 \\ \quad + 0.5\tanh\left((y - 1/3 - 0.01\sin(4\pi x))/(2\sqrt{2}\varepsilon)\right) \\ \quad - c_1(x,y,0), \\ c_3(x,y,0) = 1 - c_1(x,y,0) - c_2(x,y,0). \end{cases} \tag{27}$$

Here we use $Pe = 0.8/\varepsilon$, $Re = 5000$, $Fr = 0.8$ and the density ratio $\rho_1 : \rho_2 : \rho_3 = 0.8 : 0.9 : 1$. We omit the influence of the surface tension in this test. Fig. 10(a)–(d) are the results at the indicated time $t = 0.1$, 0.2, 0.3 and 0.45, respectively. As can be seen from the comparison, the interfacial profile satisfy the hyperbolic tangent property with the proposed model. Meanwhile, the original CH model loss more details during the interface capturing, while the modified CH model can remain.

5. Conclusion

In this study, an efficient phase-field model was established for the simulation of multi-component immiscible flows with interfacial correction in two dimension space. The influence of surface tension was well examined in the transition region. A hyperbolic Dirac function was used to smooth the deformation of interfaces between different phases. The interfacial transition was captured by a explicit smoothing flow with the modified CH equations. Furthermore, the enclosed area can be preserved by the modified CH system. Our scheme can be applied to the incompressible and immiscible fluids coupled system. The discrete system was solved by a nonlinear multi-grid method at implicit time step. We presented various numerical experiments, such as the evolution of triple junction with prescribed contact angle, shape relaxation under multi-component liquids background, convergence test with a rotate disk, deformation under shear flow, simulation of falling droplet and simulation of Kelvin–Helmholtz instability with ternary fluids, to demonstrate the efficiency and robustness of our scheme. By the comparisons between the results obtained by the original model and the modified model, we are convinced that the modification is significant during the computation of multi-component hydrodynamic system.

Declaration of competing interest

The authors declare that they have no known competing financial interests or personal relationships that could have appeared to influence the work reported in this paper.

Acknowledgments

J.S. Kim was supported by Basic Science Research Program through the National Research Foundation of Korea(NRF) funded by the Ministry of Education, Republic of Korea (NRF-2019R1A2C1003053). The corresponding author(Y.B. Li) is supported by the Fundamental Research Funds for the Central Universities, China (No. XTR042019005). The authors would like to thank the reviewers for their constructive and helpful comments regarding the revision of this article.

References

[1] J. Zhao, H. Li, Q. Wang, X. Yang, Decoupled energy stable schemes for a phase field model of three-phase incompressible viscous fluid flow, J. Sci. Comput. 70 (2017) 1367–1389.
[2] J. Yang, J. Kim, An unconditionally stable second-order accurate method for systems of Cahn–Hilliard equations, Commun. Nonlinear. Sci. 87 (2020) 105276.
[3] J. Kim, Phase field computations for ternary fluid flows, Comput. Methods Appl. Mech. Engrg. 196 (2007) 4779–4788.
[4] X. Yang, J. Zhao, Q. Wang, J. Shen, Numerical approximations for a three-component cahn-hilliard phase-field model based on the invariant energy quadratization method, Math. Mod. Meth. Appl. S 27 (2017) 1993–2030.
[5] C. Zhang, Z. Guo, Y. Li, A fractional step lattice Boltzmann model for two-phase flow with large density differences, Int. J. Heat Mass Transfer 138 (2019) 1128–1141.
[6] Y. Li, Q. Xia, C. Lee, S. Kim, J. Kim, A robust and efficient fingerprint image restoration method based on a phase-field model, 123 (2022) 108405.
[7] A.F. Brodin, D.R. Kavaliunas, S.G. Frank, Prolonged drug release from multiple emulsions, Acta Pharm. Suec. 15 (1978) 1–12.
[8] Y. Sun, C. Beckermann, Diffuse interface modeling of two-phase flows based on averaging: mass and momentum equations, Physica D 198 (2004) 281–308.
[9] Y. Li, J. Kim, Phase-field simulations of crystal growth with adaptive mesh refinement, Int. J. Heat Mass Transfer 55 (2012) 7926–7932.
[10] Y.H. Cho, J. Park, Evaluation of process parameters in the o/w/o multiple emulsion method for flavor encapsulation, J. Food Sci. J. 68 (2003) 534–538.
[11] H. Yan, M. Sedighi, H. Xie, Thermally induced diffusion of chemicals under steady-state heat transfer in saturated porous media, Int. J. Heat Mass Transfer. 153 (2020) 119664.
[12] Y. Li, L. Zhang, Q. Xia, Q. Yu, J. Kim, An unconditionally energy-stable second-order time-accurate numerical scheme for the coupled cahn-hilliard system in copolymer/homopolymer mixtures, Comput. Mater. Sci. 200 (2021) 110809.

[13] D. Eyre, Systems of Cahn–Hilliard equations, SIAM. J. Appl. Math. 53 (1993) 1686–1712.
[14] X. Yang, J. Zhao, X. He, Linear, second order and unconditionally energy stable schemes for the viscous Cahn–Hilliard equation with hyperbolic relaxation using the invariant energy quadratization method, J. Comput. Appl. Math. 343 (2018) 80–97.
[15] Y. Li, R. Liu, Q. Xia, C. He, Z. Li, First-and second-order unconditionally stable direct discretization methods for multi-component Cahn–Hilliard system on surfaces, J. Comput. Appl. Math. 401 (2022) 113778.
[16] B.D. Nichols, C.W. Hirt, Methods for calculating multidimensional, transient free surface flows past bodies, in: Proc. First Intern. Conf. Num. Ship Hydrodynamics, Gaithersburg, ML, Oct. 1975, pp. 20–23.
[17] C.W. Hirt, B.D. Nichols, Volume of fluid (VOF) method for the dynamics of free boundaries, J. Comput. Phys. 39 (1981) 201–225.
[18] M. Francois, W. shyy, Computations of drop dynamics with the immersed boundary method, part 1: numerical algorithm and buoyancy-induced effect, Numer. Heat Transfer B 44 (2003) 101–118.
[19] A.M. Roma, C.S. Peskin, M.J. Berger, An adaptive version of the immersed boundary method, J. Comput. Phys. 153 (1999) 509–534.
[20] J. Kim, D. Kim, Haecheon Choi, An immersed-boundary finite-volume method for simulations of flow in complex geometries, J. Comput. Phys. 171 (2001) 132–150.
[21] M.C. Lai, C.S. Peskin, An immersed boundary method with formal second-order accuracy and reduced numerical viscosity, J. Comput. Phys. 160 (2000) 705–719.
[22] S.J. Osher, J.A. Sethian, Fronts propagating with curvature dependent speed: algorithms based on Hamilton–Jacobi formulations, J. Comput. Phys. 79 (1988) 12–49.
[23] J. Kim, J. Lowengrub, Interfaces and Multicomponent Fluids, Encyclopedia of Mathematical Physics, Academic Press/Elsevier Science, Oxford, UK, 2006, pp. 135–144.
[24] J.S. Lowengrub, L. Truskinovsky, Quasi-incompressible Cahn–Hilliard fluids and topological transitions, Proc. R. Soc. Lond. A 454 (1998) 2617–2654.
[25] J. Kim, A generalized continuous surface tension force formulation for phase-field models for multi-component immiscible fluid flows, Comput. Methods Appl. Mech. Engrg. 198 (2009) 3105–3112.
[26] J. Kim, K. Kang, J.S. Lowengrub, Conservative multigrid methods for ternary Cahn–Hilliard systems, Commun. Math. Sci. 2 (2004) 53–77.
[27] Q. Xia, Q. Yu, Y. Li, A second-order accurate, unconditionally energy stable numerical scheme for binary fluid flows on arbitrarily curved surfaces, Comput. Method Appl. M 384 (2021) 113987.
[28] J. Kim, J. Lowengrub, Phase field modeling and simulation of three-phase flows, Int. Free Bound. 7 (2005) 435–466.
[29] J. Kim, A continuous surface tension force formulation for diffuse-interface models, J. Comput. Phys. 204 (2005) 784–804.
[30] G.I. Tóth, Phase-field theory of multicomponent incompressible Cahn-Hilliard liquids, Phys. Rev. E. 93 (2016) 013126.
[31] G.I. Tóth, Phase-field modeling of isothermal quasi-incompressible multicomponent liquids, Phys. Rev. E. 94 (2016) 033114.
[32] G.I. Tóth, T. Pusztai, L. Gránásy, A consistent multiphase-field theory for interface driven multi-domain dynamics, Phys. Rev. B 92 (2015) 184105.
[33] G.I. Tóth, J. Morris, L. Gránásy, Ginzburg–Landau type multi-phase-field model for competing fcc and bcc nucleation, Phys. Rev. L 106 (2011) 045701.
[34] J.E. Taylor, J.W. Cahn, Linking anisotropic sharp and diffuse surface motion laws via gradient flows, J. Stat. Phys. 77 (1994) 183–197.
[35] Y. Li, J. Choi, J. Kim, A phase-field fluid modeling and computation with interfacial profile correction term, Commun. Nonlinear. Sci. Numer. Simulat. 30 (2016) 84–100.
[36] F.H. Harlow, J.E. Welch, Numerical calculation of time-dependent viscous incompressible flow of fluid with free surface, Phys. Fluids 8 (1965) 2182–2189.
[37] H. Hua, J. Shin, J. Kim, Level set, phase–field, and immersed boundary methods for two–phase fluid flows, ASME J. Fluid Eng. 136 (2014) 021301.
[38] M. Sussman, P. Smereka, S. Osher, A level set approach for computing solutions to incompressible two-phase flow, J. Comput. Phys. 114 (1994) 146–159.
[39] M. Sussman, A. Almgren, J. Bell, P. Colella, L.H. Howell, M. Welcome, An adaptive level set approach for incompressible two-phase flows, J. Comput. Phys. 148 (1999) 81–124.
[40] Q. Zhang, X. Wang, Phase field modeling and simulation of three-phase flow on solid surfaces, J. Comput. Phys. 319 (2016) 79–107.
[41] C.W. Shu, S. Osher, Efficient implementation of essentially non–oscillatory shock capturing schemes II, J. Comput. Phys. 83 (1989) 32–78.
[42] J. Kim, Phase field computations for ternary fluid flows, Comput. Methods Appl. Mech. Engrg. 196 (2007) 4779–4788.
[43] Y. Li, J. Choi, J. Kim, Multi-component Cahn–Hilliard system with different boundary conditions in complex domains, J. Comput. Phys. 323 (2016) 1–16.
[44] H.G. Lee, J. Kim, An efficient numerical method for simulating multiphase flows using a diffuse interface model, Physica A 423 (2015) 33–50.
[45] H.G. Lee, J. Kim, Two-dimensional Kelvin–Helmholtz instabilities of multi-component fluids, Eur. J. Mech. B Fluids 49 (2015) 77–88.